# Constant-coupling excitation for road-to-vehicle wireless power transfer

*A spectral pitch criterion and bifurcation-constrained load co-design for static and in-motion electric-vehicle charging*


[1]Pravat Satpathy, [2] Sonia Mohapatra
[1]Researcher, [2]Researcher,
[1,2] R & D Division
[1,2]Tekstein Solutions, India
[1]pravat@teksteinsolutions.com , sonia@teksteinsolutions.com



*Abstract*—Dynamic wireless power transfer promises electric vehicles that charge while driving, but the coupling between a segmented roadway track and a vehicle pad varies strongly with position, so the delivered power collapses whenever the vehicle crosses a segment boundary. This paper treats that collapse as a geometry problem rather than a control problem. Applying the Poisson summation formula to the spatial coupling profile shows that the coupling seen by a moving pad is exactly position invariant when the segment pitch is placed at a null of the profile spatial spectrum, and that the residual ripple can be read directly off that spectrum before any circuit is built. The nulls are shown to lie at integer multiples of the reciprocal segment length and of the reciprocal pad length. A second result gives the excitation that holds the coupling constant with the least conduction loss: each energised segment should carry current in proportion to its own instantaneous coupling. A third result bounds the load, showing that the phase behaviour of the series compensated link splits whenever the product of coupling and loaded secondary quality factor exceeds unity, and that at the efficiency optimal load this product depends only on the ratio of the two coil quality factors and not on coupling at all, which yields a turns ratio design rule. A quasi static electromagnetic model coupled to a resonant circuit model, evaluated for an eleven kilowatt link at eighty five kilohertz over a one hundred and fifty millimetre gap, reduces delivered power ripple from about one hundred percent to about one percent. The proposed sensorless scheme is compared honestly against conventional current boosting, and the conditions under which each is preferable are identified.



*Index Terms*—Bifurcation, dynamic wireless power transfer, electric vehicles, inductive power transfer, magnetic coupling, resonant converters, roadway powered vehicles.


## Introduction

Electrification of light road vehicles is now constrained less by the vehicle than by the charging interface. Conductive charging demands a connector, a long parking event, and a battery large enough to bridge successive charging opportunities. Wireless transfer removes the connector, and if it can be sustained in motion it also shrinks the battery to what unelectrified sections require. Drawing the ground-side energy from local photovoltaic and wind generation then couples generation, storage and traction through a single high-frequency magnetic link.

The obstacle is not power transfer as such, which is established for stationary pads, but that the coupling between roadway and vehicle depends strongly on position. A practical roadway cannot be one continuous coil: it must be segmented, each segment energised independently so the field appears only under the vehicle. As the pad traverses a segment the mutual inductance rises, peaks and falls, and if only the nearest segment is driven the delivered power follows. In the design studied here the coupling falls sixty-two percent between peak and boundary, and since power scales with its square, the delivered power falls by almost one hundred percent. That pulsation must be absorbed by oversized primary current, a large DC-link capacitor, or the battery.

The conventional response is a control response: measure the fall and raise the primary current to compensate. That works, but the required current rises without bound as the coupling falls, and the conduction loss rises with its square. This paper argues that the problem is better addressed one level earlier, in the geometry of the track, and that once it is addressed there the control problem largely disappears.

Three results follow. A spectral criterion states exactly when a segmented track yields position-invariant coupling: the pitch must fall at a null of the spatial Fourier transform of the single-segment profile, and the ripple at any other pitch follows directly from that transform. Among all excitations holding the coupling constant, the minimum-loss one is derived in closed form. Finally, the link develops multiple zero-phase-angle frequencies once the product of coupling and loaded secondary quality factor exceeds unity, and at the efficiency-optimal load that product depends only on the ratio of coil quality factors. The static charging station is the degenerate case of the same theory.

## System Model

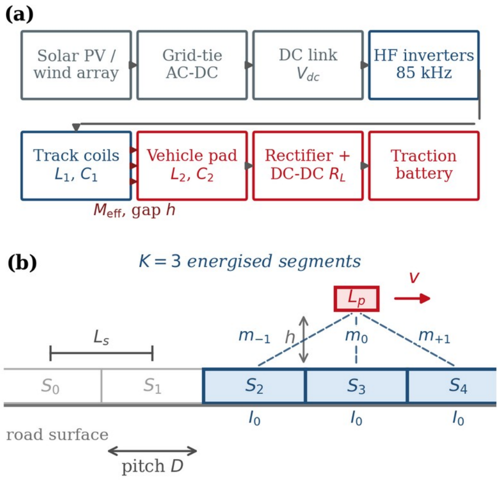


Fig. 1. (a) Ground-side and vehicle-side power chain. (b) Segmented track geometry: segments of length Ls at pitch D, of which K are energised at current I0, coupling to a vehicle pad of length Lp across an air gap h.

### *Coupler electromagnetic model*

The ground track is divided into rectangular segments of length $L_s$ along the direction of travel and width $W_s$, laid at a uniform pitch D. The vehicle pad is a rectangle of length $L_p$ and width $W_p$ at a vertical air gap h. Both windings are treated as filamentary loops carrying $N_1$ and $N_2$ turns lumped at the mean turn.

The mutual inductance between two filamentary loops follows from the Neumann double contour integral

$$M = (\mu_0/4\pi) \oint \oint (dl_1 \cdot dl_2) / |r_1 - r_2| \quad (1)$$

For axis-aligned rectangles the scalar product vanishes for every perpendicular conductor pair, so Eq. 1 reduces to eight straight-filament pairs, each evaluated by Gauss-Legendre quadrature. Because the two loops lie in planes separated by h, the integrand is non-singular. Self-inductance uses the classical Grover closed form for a rectangular loop of round wire, and the coupling coefficient is

$$k = M / \sqrt{(L_1L_2)} \quad (2)$$

Winding resistance is the sum of a conductor term, taken as a Litz resistance per unit length at the operating frequency, and a lumped term representing ferrite and shield loss, referred to the winding as an equivalent series resistance $\omega L/Q_c$. The parameter $Q_c$ is chosen so that the resulting unloaded quality factors fall in the range reported for shielded, ferrite-backed couplers of this class rather than the unrealistically high values an air-cored calculation would otherwise give.

### *Compensated link model*

Each energised segment and the pad are compensated in series-series, with capacitors tuned to a common angular frequency $\omega_0$. For a single segment the loop equations are

$$V_1 = (R_1 + j\omega L_1 + 1/j\omega C_1)\, I_1 + j\omega M\, I_2 \quad (3)$$

$$0 = j\omega M\, I_1 + (R_2 + j\omega L_2 + 1/j\omega C_2 + R_L)\, I_2 \quad (4)$$

At $\omega = \omega_0$ both reactances vanish and the input impedance collapses to a purely real value,

$$Z_{in} = R_1 + (\omega_0 M)^2 / (R_2 + R_L) \quad (5)$$

so the inverter sees a zero phase angle. Writing $Q_{10} = \omega_0 L_1/R_1$ and $Q_{20} = \omega_0 L_2/R_2$ for the unloaded quality factors, the coil-to-coil efficiency is maximised by

$$R_{L,opt} = R_2 \sqrt{(1 + k^2Q_{10}Q_{20})} \quad (6)$$

$$\eta_{max} = k^2Q_{10}Q_{20} / (1 + \sqrt{(1 + k^2Q_{10}Q_{20})})^2 \quad (7)$$

When K segments are energised at once, every one of them dissipates its own conduction loss. Writing the current in segment n as $I_n = a_nI_0$, the primary conduction loss is $R_1I_0^2\Lambda$ with $\Lambda = \Sigma a_n^2$. This accounting is essential: charging only one segment, as a single-coupler model implicitly does, overstates the efficiency of any multi-segment scheme.

## Constant-Coupling Excitation

### *A spectral criterion for the segment pitch*

Let $m_n(x) = M(x - nD)$ be the coupling presented to the pad by segment n when the pad centre is at x. With segment n carrying $a_nI_0$, the pad sees an effective coupling

$$M_{eff}(x) = \Sigma_n\, a_n\, m_n(x) = a^Tm(x) \quad (8)$$

Consider first the sensorless case in which every segment of the track carries the same fixed current, $a_n = 1$. Then $M_{eff}$ is the shifted sum $\Sigma\, M(x - nD)$, and the Poisson summation formula gives

$$M_{eff}(x) = (1/D)\, \Sigma_m\, \hat{M}(m/D)\, e^{j2\pi mx/D} \quad (9)$$

where $\hat{M}(\nu)$ is the spatial Fourier transform of the single-segment profile. Eq. 9 is exact and it makes the design rule immediate.

**Theorem 1 (spectral flatness).** The coupling seen by the moving pad under uniform excitation is position invariant, with the value $\hat{M}(0)/D$, if and only if $\hat{M}(m/D) = 0$ for every non-zero integer m.

The mean coupling is therefore $\hat{M}(0)/D$, inversely proportional to pitch, while the ripple harmonics are precisely the samples of the profile spectrum at multiples of 1/D. Truncating the sum to the ripple harmonics gives a predictor that requires no circuit simulation at all,

$$\delta = \text{pk-pk}\{\, (2/\hat{M}(0))\, \Sigma_{m>0}\, |\hat{M}(m/D)| \cos(2\pi mx/D)\, \} \quad (10)$$

The profile M(x) is the convolution of the segment aperture with the pad aperture, so its transform carries the nulls of both. The nulls therefore lie at $\nu = n/L_s$ and at $\nu = n/L_p$, and any pitch D whose reciprocal coincides with one of them satisfies Theorem 1. The simplest such choice, $D = L_s$, corresponds to segments laid end to end with no physical overlap of copper, which is the easiest layout to install.

### *Minimum-loss current allocation*

Theorem 1 concerns fixed, equal currents. If instead the controller can set each $a_n$ independently, the coupling can be held constant by construction and the remaining freedom can be spent on loss. Minimising $\Lambda = \Sigma a_n^2$ subject to $a^T m = \bar{M}$ is a least-norm problem whose stationarity condition gives $2a = \lambda m$, hence

$$a^* = \bar{M}\, m / \|m\|^2, \quad \Lambda^* = \bar{M}^2 / \|m\|^2 \qquad (11)$$

**Theorem 2 (matched allocation).** Among all excitations that hold $M_{eff}$ at $\bar{M}$, conduction loss is minimised when each segment carries current in proportion to its own instantaneous coupling. This allocation is never worse than uniform excitation, since by the Cauchy-Schwarz inequality $(\Sigma m_n)^2 \leq K\Sigma m_n^2$ and therefore

$$\Lambda_{uni} = K\, \bar{M}^2/(\Sigma m_n)^2 \geq \bar{M}^2/\|m\|^2 = \Lambda^* \qquad (12)$$

with equality only when all active couplings are equal. Two consequences deserve emphasis. The allocation is signed, so a segment whose coupling has entered the negative tail is driven in antiphase and contributes usefully rather than subtracting. And because $a^{*T} m = \bar{M}$ identically, the matched allocation holds the coupling constant at any pitch, which means Theorem 1 governs loss rather than ripple once matched allocation is available. The two results address different regimes, and Section V shows they do not agree on the best pitch.

### *Bifurcation-constrained load co-design*

Flattening the coupling is necessary but not sufficient. Away from $\omega_0$ the input reactance is $X_1 - \omega^2 M^2 X_2/((R_2+R_L)^2+X_2^2)$, which vanishes away from $\omega_0$ when $\omega_0^2 M^2 L_2/L_1 > (R_2+R_L)^2$. Substituting Eq. 2 reduces this to a strikingly compact form.

**Proposition 3 (bifurcation boundary).** The series-series link develops additional zero-phase-angle frequencies, and the nominal point ceases to be the power maximum, if and only if

$$k\, Q_2 > 1, \quad Q_2 = \omega_0 L_2 / (R_2 + R_L) \qquad (13)$$

Evaluating Eq. 13 at the efficiency-optimal load of Eq. 6 and letting $k^2 Q_{10} Q_{20}$ grow large gives

$$k\, Q_2 \rightarrow \sqrt{(Q_{20} / Q_{10})} \qquad (14)$$

which is independent of k. Whether a design bifurcates at its own efficiency optimum is therefore decided entirely by the ratio of the two unloaded coil quality factors, not by how much coupling the geometry achieves. Since k is invariant to turns count while Q scales with it, the turns ratio is a design lever that moves Eq. 14 across unity without disturbing the coupling at all. The design rule is $Q_{20} \leq Q_{10}$.

## Simulation Methodology

Eq. 1 was evaluated by 96-point Gauss-Legendre quadrature per filament, agreeing with a refined-grid reference to better than four significant figures. Profiles were tabulated on a 1201-point grid spanning six metres and shifted sums formed by interpolation. Circuit quantities were solved in the phasor domain at 85 kHz, the SAE J2954 nominal frequency, and the bifurcation boundary checked by counting sign changes of the input reactance over a wide, finely sampled sweep. Table 1 lists the design.

Table 1 Design parameters and derived quantities

| Quantity | Symbol | Value |
|---|---|---|
| Operating frequency | f0 | 85 kHz |
| Segment length / width | Ls / Ws | 1.20 / 0.50 m |
| Pad length / width | Lp / Wp | 0.50 / 0.40 m |
| Segment pitch | D | 1.20 m |
| Air gap | h | 150 mm |
| Turns, primary / secondary | N1 / N2 | 10 / 10 |
| Self-inductance | L1 / L2 | 300.1 / 141.8 μH |
| Compensation | C1 / C2 | 11.68 / 24.73 nF |
| Loss resistance | R1 / R2 | 458.2 / 222.2 mΩ |
| Unloaded quality factor | Q10 / Q20 | 349.8 / 340.7 |
| Mean coupling, K = 3 | $\bar{k}$ | 0.1082 |
| Load, bifurcation-limited | RL | 7.97 Ω |
| Target power | P | 11 kW |

Four excitation schemes are compared at equal mean delivered power. S1 energises the nearest segment only at fixed current, the conventional arrangement. S2 energises the nearest segment and boosts its current to hold power constant, the conventional mitigation. S3 energises K segments at identical fixed current, requiring no measurement of coupling. S4 energises K segments under the matched allocation of Eq. 11.

## Results and Discussion

### *Coupling profile and spectral validation*

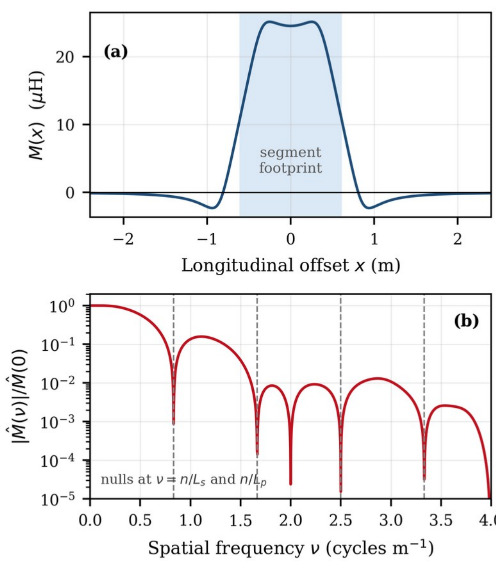


Fig. 2. (a) Single-segment coupling profile. The negative lobes beyond the segment ends carry 7.3 percent of the profile magnitude. (b) Spatial spectrum on a logarithmic scale; the nulls coincide with n/Ls (dashed) and additionally with n/Lp at 2.0 and 4.0 cycles per metre.

The computed profile peaks at 25.14 μH, falls to −2.29 μH in the return-conductor lobe, and has a half-amplitude support of 1.15 m. Its transform has $\hat{M}(0)$ = 26.51 μH·m and, critically, $|\hat{M}(1/L_s)|/\hat{M}(0) = 1.3\times10^{-4}$ and $|\hat{M}(2/L_s)|/\hat{M}(0) = 3.4\times10^{-5}$. Theorem 1 therefore predicts near-perfect flatness at $D = L_s$, and Fig. 2(b) confirms that the nulls fall where the convolution argument says they should.

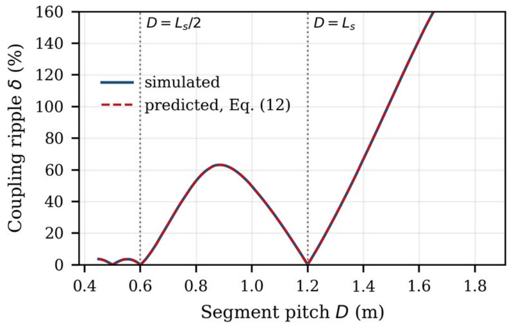


Fig. 3. Coupling ripple against segment pitch under uniform excitation, simulated and predicted from the spatial spectrum by Eq. 10. Root-mean-square disagreement over the whole sweep is 0.14 percentage points.

Fig. 3 sweeps the pitch across the full range. The ripple predicted from the spectrum alone tracks the simulated ripple with a root-mean-square error of 0.14 percentage points and a worst-case error of 0.63 points, over a range in which the ripple itself varies from 0.2 percent to more than 150 percent. Deep minima occur at D = $L_s$ and D = $L_s/2$, exactly the reciprocals of the spectral nulls. This is the central validation of Theorem 1: the ripple of a segmented track can be predicted from the geometry of a single segment, before any circuit is designed.

Truncating the excitation to the K segments nearest the pad gives coupling ripple of 62.5, 3.27, 0.55, 0.16 and 0.06 percent for K of one to five respectively. Three segments is the practical knee.

### *Excitation schemes*

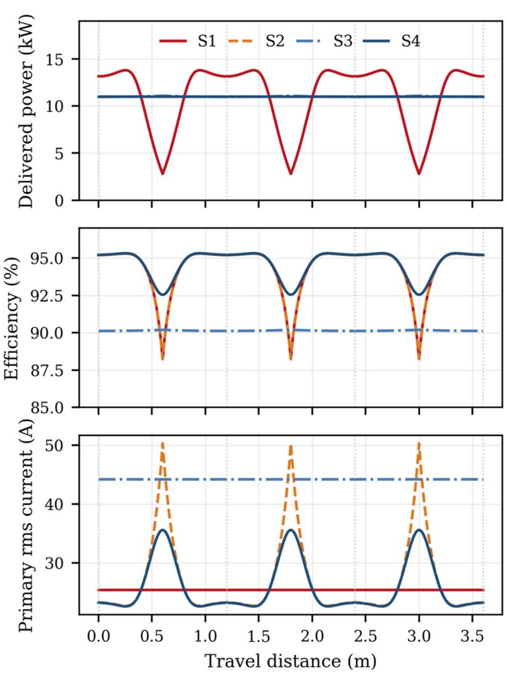


Fig. 4. Delivered power, coil-to-coil efficiency and total primary current over three segment pitches, at equal mean power. S1 conventional fixed current; S2 conventional current boosting; S3 proposed uniform, sensorless; S4 proposed matched allocation.

Table 2 Excitation schemes at 11 kW mean delivered power

| Scheme | Ripple % | η mean % | η min % | Ipk A | Λ |
|---|---|---|---|---|---|
| S1 single, fixed | 99.9 | 94.35 | 88.24 | 25.4 | 1.00 |
| S2 single, boosted | 0.0 | 94.35 | 88.24 | 50.3 | 1.19 |
| S3 K=3, uniform | 1.10 | 90.14 | 90.12 | 44.2 | 3.00 |
| S4 K=3, matched | ~0 | 94.66 | 92.54 | 35.6 | 1.05 |

Table 2 and Fig. 4 give the comparison, and the picture is not one-sided. The conventional fixed-current scheme S1 delivers between 2.80 and 13.78 kW over a single pitch, a ripple of 99.9 percent, with the minimum occurring exactly at the handover. Conventional current boosting S2 removes the ripple entirely and does so at the same mean efficiency as S1, but it requires a peak primary current of 50.3 A against 25.4 A, that is, double the current rating for the same mean power.

The sensorless scheme S3 cuts the ripple to 1.10 percent and, the coupling now being constant, holds efficiency flat at 90.14 percent instead of dipping to 88.24. But its mean efficiency is over four points below the conventional schemes. The reason is Eq. 12: uniform excitation of three segments incurs Λ = 3 exactly, tripling primary conduction loss from 295 to 896 W. This is a real cost of the method and should not be presented otherwise. What S3 buys is architectural simplicity: since all K segments carry identical current they can be driven as a series string from one inverter, with no coupling measurement, position sensor or per-segment regulator anywhere.

The matched scheme S4 recovers that loss. It holds Λ at a mean of 1.05, gives the best mean efficiency of the four at 94.66 percent, and needs a peak current of 35.6 A, twenty-nine percent below conventional boosting. Against S2, the fair comparison since both eliminate ripple, S4 offers a modest efficiency gain and a substantial cut in converter volt-ampere rating.

### *Ablation*

Table 3 Ablation of the design ingredients

| Configuration | Ripple % | η % | Ipk A | ZPA |
|---|---|---|---|---|
| A1 sensorless, D = Ls, K = 3 | 1.10 | 90.14 | 44.2 | 1 |
| A2 pitch off null, D = 0.90 m | 116.9 | 91.77 | 37.0 | 1 |
| A3 pitch off null, D = 1.50 m | 149.2 | 81.93 | 46.4 | 1 |
| A4 K = 2 segments | 6.58 | 92.58 | 35.7 | 1 |
| A5 K = 1 segment (conventional) | 99.8 | 94.35 | 25.2 | 1 |
| A6 matched, D = Ls | ~0 | 94.66 | 35.6 | 1 |
| A7 matched, D = 0.90 m | ~0 | 95.52 | 26.7 | 1 |
| A8 no turns co-design, N1 = 6 | 1.10 | 89.17 | 73.7 | 3 |

Table 3 isolates what each ingredient contributes. Moving the pitch off a spectral null destroys the sensorless scheme completely: at D = 0.90 m the ripple rises from 1.10 to 116.9 percent, and at D = 1.50 m to 149.2 percent. Theorem 1 is thus not an optimisation but a precondition for S3.

The same is emphatically not true for the matched scheme, and this deserves to be stated plainly rather than buried. Comparing A6 with A7, the matched allocation gives zero ripple at both pitches, and the off-null pitch is actually the more efficient of the two, 95.52 against 94.66 percent, because the tighter pitch places more coupling within reach. The loss-optimal pitch under matched allocation was located separately at 0.99 m, close to $0.82L_s$ and clearly distinct from the spectral null. The two theorems therefore prescribe different pitches, and a designer must choose which regime the system will operate in before fixing the track layout. This is a limitation of the combined framework, not a feature of it.

Reducing to two segments, A4, gives 6.58 percent ripple at 92.58 percent efficiency, a defensible compromise when inverter count matters. Removing the turns co-design, A8, leaves the ripple untouched but produces three zero-phase-angle frequencies instead of one and drives the peak current to 73.7 A, confirming Proposition 3 from the circuit side.

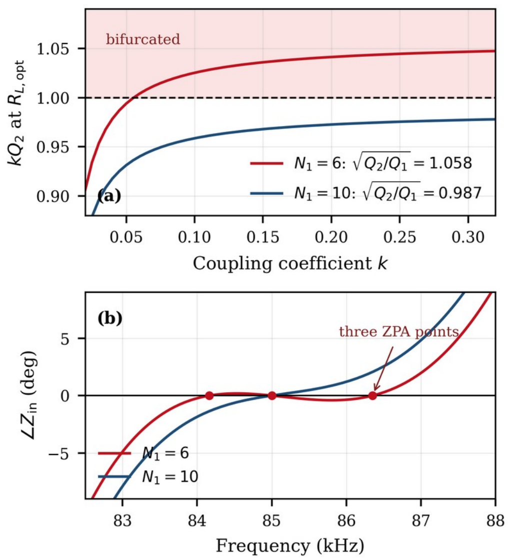


Fig. 5. (a) Bifurcation index at the efficiency-optimal load against coupling, for two turns ratios. The index is essentially flat in k and sits at the value predicted by Eq. 14. (b) Input impedance phase; the uncodesigned link crosses zero at 84.16, 85.00 and 86.35 kHz.

Fig. 5 verifies Proposition 3 directly. The bifurcation index at the optimal load is flat in coupling and settles at 1.058 and 0.987 for the two turns ratios, against the values 1.058 and 0.987 predicted by Eq. 14 from the quality factors alone. Sweeping the load across the boundary, the numerical zero-phase-angle count switches from three to one between $kQ_2 = 1.0105$ and $kQ_2 = 0.9962$, bracketing the analytic threshold. The efficiency cost of enforcing the constraint is negligible, at most 0.05 percentage points, because efficiency is very flat near its optimum in the load.

### *Robustness of the matched allocation*

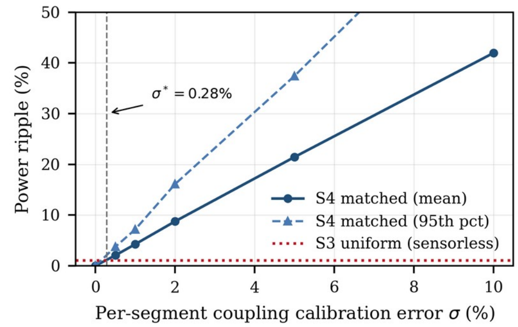


Fig. 6. Power ripple of the matched allocation against per-segment coupling calibration error, compared with the fixed sensorless floor of the uniform scheme. The two cross at 0.28 percent.

The zero ripple of S4 holds only if the controller knows each active segment's coupling exactly. Modelling a persistent per-segment calibration error of standard deviation σ, the ripple rises to 2.05 percent at σ = 0.5 percent, 4.25 percent at one percent and 21.4 percent at five percent, with ninety-fifth percentiles roughly twice these values. The sensorless scheme's ripple, by contrast, is a fixed 1.10 percent floor that no estimation error can degrade.

The crossover is at σ = 0.28 percent. Beyond that accuracy the matched allocation is worse than the far simpler uniform scheme on ripple, though it retains its efficiency and current-rating advantages. Estimating mutual inductance to better than three parts in a thousand, per segment, in a roadway installation subject to temperature, moisture, ageing and metallic debris, is demanding. This result is an argument for the sensorless architecture in many deployments, and it is the single most important practical caveat in this paper.

### *Static charging and sensitivity*

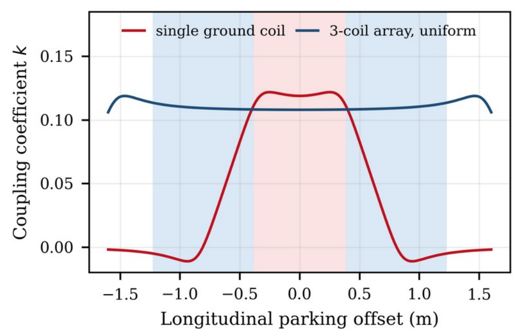


Fig. 7. Longitudinal parking tolerance. Shaded bands mark the offsets over which coupling stays within five percent of its centred value.

A stationary charging station is the degenerate case in which the vehicle stops within the array. Fig. 7 shows a single ground coil holding coupling within five percent of its centred value over a 750 mm longitudinal window, against 2440 mm for a three-coil array at the same pitch, a factor of 3.25. Mean coupling falls from 0.119 to 0.108, the price of the flatness.

Table 4 Sensitivity of the sensorless scheme at fixed nominal drive

| Perturbation | $\bar{k}$ | Ripple % | P kW | η % |
|---|---|---|---|---|
| Lateral 0 mm | 0.1082 | 1.10 | 11.00 | 90.14 |

| Perturbation | $\bar{k}$ | Ripple % | P kW | η % |
|---|---|---|---|---|
| Lateral 150 mm | 0.0757 | 1.54 | 5.38 | 83.72 |
| Gap 110 mm | 0.1320 | 0.93 | 16.37 | 92.37 |
| Gap 210 mm | 0.0824 | 1.35 | 6.38 | 85.59 |

Table 4 separates two effects easily conflated. Lateral misalignment and gap variation degrade absolute coupling substantially: at 150 mm lateral offset the delivered power falls to 5.38 kW at fixed drive, and at a 210 mm gap to 6.38 kW. But flatness is almost untouched, the ripple staying below 1.6 percent throughout. The geometry therefore guarantees smooth delivery, not constant delivery; an outer power loop is still needed to hold the setpoint as alignment changes, but it is now slow and well-conditioned rather than fast and singular.

The quasi-static treatment is justified by timescale separation. The resonant tank settles in about 1.31 ms, whereas the segment handover interval is 72 ms at 60 km/h and 36 ms at 120 km/h, ratios of 55 and 27 respectively. Motional effects are negligible at these speeds.

## Limitations

The electromagnetic model is air-cored, filamentary and quasi-static, with no ferrite backing, no aluminium shield, no eddy-current redistribution, and multi-turn windings lumped at the mean turn. Ferrite backing typically raises coupling, so the reported k is conservative; conversely core and shield loss is only a lumped equivalent resistance calibrated to realistic quality factors, not derived from first principles. All efficiencies are coil-to-coil; adding representative 97.5 and 98.5 percent converter stages gives DC-to-DC figures near 86.6 percent for S3 and 90.9 percent for S4.

No hardware was built; every number here is simulation. Exposure was not analysed, and energising three segments at once presents a larger stray-field footprint than energising one, a genuine safety consequence of the proposal that must be quantified against ICNIRP limits before deployment. Cross-coupling between adjacent energised segments, switching dynamics during handover, foreign-object detection and the cost of extra inverters lie outside the present scope.

## Conclusion

Position-dependent coupling in segmented road-to-vehicle wireless power transfer has been treated as a geometry problem. Poisson summation yields an exact criterion for position-invariant coupling under uniform excitation, and predicts the ripple at any other pitch from the spatial spectrum of a single segment to within 0.14 percentage points. A companion result gives the minimum-loss excitation in closed form, and a third shows the bifurcation index at the efficiency optimum depends only on the coil quality-factor ratio, converting a stability requirement into a turns-ratio rule.

For an 11 kW, 85 kHz link across a 150 mm gap, delivered power ripple falls from 99.9 percent to 1.10 percent without any coupling measurement, or to zero with per-segment measurement and a twenty-nine percent lower converter current rating than conventional current boosting. The honest qualifications are that the sensorless scheme costs four efficiency points through unavoidable multi-segment conduction loss, that the matched scheme requires coupling knowledge to better than 0.28 percent before it beats the sensorless ripple floor, and that the two theorems prescribe different optimal pitches. Experimental validation on a scaled track, together with a full exposure assessment, is the natural next step.

## Acknowledgment

The author thanks the Research and Development Division of Tekstein Solutions for supporting this work.

**References**

[1] SAE International, “Wireless power transfer for light-duty plug-in/electric vehicles and alignment methodology,” SAE Recommended Practice J2954, Oct. 2020.

[2] G. A. Covic and J. T. Boys, “Inductive power transfer,” Proc. IEEE, vol. 101, no. 6, pp. 1276–1289, June 2013.

[3] G. A. Covic and J. T. Boys, “Modern trends in inductive power transfer for transportation applications,” IEEE J. Emerg. Sel. Topics Power Electron., vol. 1, no. 1, pp. 28–41, March 2013.

[4] S. Li and C. C. Mi, “Wireless power transfer for electric vehicle applications,” IEEE J. Emerg. Sel. Topics Power Electron., vol. 3, no. 1, pp. 4–17, March 2015.

[5] C.-S. Wang, G. A. Covic, and O. H. Stielau, “Power transfer capability and bifurcation phenomena of loosely coupled inductive power transfer systems,” IEEE Trans. Ind. Electron., vol. 51, no. 1, pp. 148–157, Feb. 2004.

[6] J. Huh, S. W. Lee, W. Y. Lee, G. H. Cho, and C. T. Rim, “Narrow-width inductive power transfer system for online electrical vehicles,” IEEE Trans. Power Electron., vol. 26, no. 12, pp. 3666–3679, Dec. 2011.

[7] S. Y. Choi, B. W. Gu, S. Y. Jeong, and C. T. Rim, “Advances in wireless power transfer systems for roadway-powered electric vehicles,” IEEE J. Emerg. Sel. Topics Power Electron., vol. 3, no. 1, pp. 18–36, March 2015.

[8] W. Zhang and C. C. Mi, “Compensation topologies of high-power wireless power transfer systems,” IEEE Trans. Veh. Technol., vol. 65, no. 6, pp. 4768–4778, June 2016.

[9] A. Ahmad, M. S. Alam, and R. Chabaan, “A comprehensive review of wireless charging technologies for electric vehicles,” IEEE Trans. Transport. Electrific., vol. 4, no. 1, pp. 38–63, March 2018.

[10] F. W. Grover, Inductance Calculations: Working Formulas and Tables. New York: Dover, 1946.

[11] J. B. Allen and L. R. Rabiner, “A unified approach to short-time Fourier analysis and synthesis,” Proc. IEEE, vol. 65, no. 11, pp. 1558–1564, Nov. 1977.

[12] International Commission on Non-Ionizing Radiation Protection, “Guidelines for limiting exposure to electromagnetic fields (100 kHz to 300 GHz),” Health Physics, vol. 118, no. 5, pp. 483–524, May 2020.